Supplement 1: Entheseal Patterns Suggest Habitual Tool Use in Early Hominins

JANA KUNZE
Paleoanthropology, Senckenberg Centre for Human Evolution and Palaeoenvironment, Institute for Archaeological Sciences, Eberhard Karls University of Tübingen, Tübingen, GERMANY; jana.kunze@uni-tuebingen.de

FOTIOS ALEXANDROS KARAKOSTIS*
DFG Centre of Advanced Studies 'Words, Bones, Genes, Tools' Eberhard Karls University of Tübingen, Tübingen, GERMANY; fotios-alexandros.karakostis@uni-tuebingen.de

STEFAN MERKER
Department of Zoology, State Museum of Natural History Stuttgart, Stuttgart, GERMANY; stefan.merker@smns-bw.de

MARCO PERESANI
Deparment of Humanities, Section of Prehistoric and Anthropological Sciences, University of Ferrara, Ferrara; and, Institute of Environmental Geology and Geoengineering, National Research Council, Milano, ITALY; psm@unife.it

GERHARD HOTZ
Anthropological Collection, Natural History Museum of Basel, Basel; and, Integrative Prehistory and Archaeological Science, University of Basel, Basel, SWITZERLAND; Gerhard.Hotz@bs.ch

VANGELIS TOURLOUKIS
Paleoanthropology, Senckenberg Centre for Human Evolution and Palaeoenvironment, Institute for Archaeological Sciences, Eberhard Karls University of Tübingen, Tübingen, GERMANY; vangelis.tourloukis@ifu.uni-tuebingen.de

KATERINA HARVATI*
Paleoanthropology, Senckenberg Centre for Human Evolution and Palaeoenvironment, Institute for Archaeological Sciences, Eberhard Karls University of Tübingen, Tübingen; and, DFG Centre of Advanced Studies 'Words, Bones, Genes, Tools' Eberhard Karls University of Tübingen, Tübingen, GERMANY; katerina.harvati@ifu.uni-tuebingen.de

SUPPLEMENT 1

OVERALL 1ST METACARPAL SHAPE

We combined the analysis of entheseal patterns with a 3D geometric morphometric analysis of standard functional morphology in the overall bone shape, including the first metacarpal's diaphysis, articular surfaces, and three muscle attachment sites (e.g., Karakostis et al. 2018). In contrast to entheseal proportions, which focus on proportionate size (i.e., surface area) and are analyzed to reconstruct habitual activity (Castro et al. 2021; Karakostis et al. 2017; Karakostis et al. 2019a; 2019b; Karakostis and Harvati 2021), entheseal shape has been associated with muscle force-producing efficiency. For example, in previous biomechanical modeling research (Karakostis et al. 2020; 2021), a more relatively projecting OP attachment site has shown to significantly increase joint moment arms for flexion, and thus the force-producing efficiency, of the attaching muscle.

METHODS

Statistical analysis

To analyze all aspects of overall metacarpal shape together, the 37 landmarks were combined in one .nts file per individual and then imported into RStudio (RStudio Inc., Boston; R version 3.6.2 for Windows, R Core Team 2021). There, the landmark coordinates were Procrustes superimposed by rotation, centering, and scaling. The resulting Procrustes coordinates of the comparative sample were then analyzed in a shape Principal Component Analysis, an analysis with no *a priori* group assumptions. The scree-plot approach was used to determine the number of relevant PCs for plotting and further analysis (Field 2017). Subsequently, the PC scores of the early fossil hominins were calculated in R using the 'predict' function and then projected onto the PC plot. The absence of outliers was visually confirmed.

Precision test

All landmarks of six individuals were digitized a second time by the same observer (JK) a month after the first digitization (see precision test in the main article). The error between repetitions was analyzed using the Centroid Radius approach. This method measures the Euclidian distance between the landmark repetitions and their centroid, which is calculated based on the provided landmark configurations (Cramon-Taubadel et al. 2007; Singleton 2002). Thereby, the deviation between repetitions can be calculated for each landmark separately. The digitization error was consistently below 5% for all landmarks with a maximum error of 3.4% and a mean error of 0.32%.

RESULTS AND DISCUSSION

The results of the morphological analysis of shape involving functional morphological characters are illustrated in Figure 3 and SOM Figure 1. In the former, PC1 is plotted against PC2, while the latter includes PC3 on the y-axis. Here, we mainly focus on the PC plot including PC3 (see Figure 3), as the shape variation depicted on this axis is more relevant for the purposes of this study. Additionally, this Principal Component shows better separation of taxa than PC2. The shape differences represented along PC1 (52.08% of variance, SOM Table 5) comprise morphological characters (captured by our landmark configurations; Methods, see Figure 2, SOM Table 4) widely interpreted as indicators of efficiency—metacarpal robusticity (Ruff et al. 2006); width and curvature of the distal articular surface (Galletta et al. 2019); dorsoventral curvature of the proximal articular surface (Marchi et al. 2017; Marzke et al. 2010); the degree of distal extension of the DI1 enthesis (Jacofsky 2009; Tocheri et al. 2008); proximal extension and lateral projection of the OP attachment site (Karakostis et al. 2020; 2021; Maki and Trinkaus 2011). PC3 (7.28 % of total variance), on the other hand, reflects changes in metacarpal robusticity, elongation of the DI1 enthesis, shape of the APL attachment site, OP lateral projection, dorsopalmar length of the proximal articular surface, and medial extension of the distal articular surface and head asymmetry. Finally, the shape variation on PC2 (14.65% of variance) is mainly driven by the proximal extension of the OP enthesis, but also reflects orientation of the DI1 (palmar-dorsal) and APL entheses (proximal-distal) and dorsoventral curvature of the proximal articular surface (see SOM Figure 1).

PC1 shows a clear separation between *H. sapiens* / *H. neanderthalensis* and the great apes, with only slight overlapping between later *Homo* and *Pan* (one specimen, likely driven by a distally extending DI1 enthesis), while PC3 separates *Gorilla* from *Pan* and *Pongo*. On PC2 on the other hand, there is an extensive overlap among all groups. The early fossil hominins (projected onto the PC plot) are more widely dispersed than in the analysis of entheseal proportions. While SK 84 plots with *H. sapiens* / *H. neanderthalensis* with a positive PC1 score, all *Australopithecus* specimens, including *A. sediba*, are characterized by more negative scores, plotting away from later hominins and at the margins of the *Pan* convex hull. Although *H. naledi* overlaps with the other *Homo* samples on PC1, it shows an extreme negative PC3 score, thus occupying a unique position on the plot. This can at least partially be explained by its unusually small proximal articular surface.

The shape analysis revealed patterns of variation that directly reflect morphological characters widely associated with manual mechanical capacity. Compared to great apes, modern humans and Neanderthals showed a robust thumb metacarpal, usually seen as an adaptation to increased load on this bone (Kivell 2015; Ruff et al. 2006); a wide and flat distal articular surface, associated with increased stability of the metacarpophalangeal joint to increase the load resistance of the thumb during forceful precision grips (Galletta et al. 2019); and a dorsoventrally flatter proximal articular surface that provides higher mobility of the trapeziometacarpal joint (Marchi et al. 2017; Marzke et al. 2010) (see shape changes in Figure 2 and SOM Figure 1). Due to their functional importance, these characteristics are commonly associated with efficient human-like tool production and use. Importantly, our analysis shows these highly functional features co-occurring with distinct, functionally relevant, entheseal shapes, including a distally extending DI1 and a laterally projecting OP enthesis, in both Neanderthals and modern humans. A histological study on DI1 (Jacofsky 2009) and recent modelling work on OP (Karakostis et al. 2021) have linked these characteristics with a larger joint moment arm, and therefore greater efficiency for the attaching muscles (Karakostis et al. 2018; 2020; 2021; Maki and Trinkaus 2011; Tocheri et al. 2008). We therefore interpret the results of our combined shape analysis as reflecting adaptations to biomechanical efficiency. In contrast to the entheseal proportion analysis, earlier hominins did not all share these biomechanically important features with later *Homo*, indicating that only some of the taxa examined here had evolved these biomechanical adaptations. Despite their human-like entheseal proportions, both *A. afarensis* and *A. sediba* present an overall bone morphology similar to *Pan* and *Pongo* and therefore likely experienced low manual dexterity compared to later *Homo*. Although *A. africanus* appears to differ in morphology from the other two australopiths, it also shows an overall bone shape more similar to that of great apes. In contrast, the overall morphology of SK 84 clearly reflects a human-like biomechanical adaptation, and the bone and entheseal shape of *H. naledi* is the most distinct from that of great apes in the entire sample.

REFERENCES

Castro, A.A., Karakostis, F.A., Copes, L.E., McClendon, H.E., Trivedi, A.P., Schwartz, N.E., Garland, T., 2021. Effects of selective breeding for voluntary exercise, chronic exercise, and their interaction on muscle attachment site morphology in house mice. *J. Anat.* 240(2), 279–295.

Cramon-Taubadel, N. von, Frazier, B.C., Lahr, M.M., 2007. The problem of assessing landmark error in geometric morphometrics: theory, methods, and modifications. *Am. J. Phys. Anthropol.* 134(1), 24–35.

Field, A., 2017. *Discovering Statistics Using IBM SPSS Sta-*

tistics, 5th ed. Sage Publications, Thousand Oaks, CA.

Galletta, L., Stephens, N.B., Bardo, A., Kivell, T.L., Marchi, D., 2019. Three-dimensional geometric morphometric analysis of the first metacarpal distal articular surface in humans, great apes and fossil hominins. *J. Hum. Evol.* 132, 119–136.

Jacofsky, M.C., 2009. *Comparative Muscle Moment Arms of the Primate Thumb: Homo, Pan, Pongo, and Papio*. Ph.D. Dissertation, Arizona State University.

Karakostis, F.A., Haeufle, D., Anastopoulou, I., Moraitis, K., Hotz, G., Tourloukis, V., Harvati, K., 2021. Biomechanics of the human thumb and the evolution of dexterity. *Curr. Biol.* 31(6), 1317–1325.e8.

Karakostis, F.A., Harvati, K., 2021. New horizons in reconstructing past human behavior: introducing the "Tübingen University Validated Entheses-based Reconstruction of Activity" method. *Evol. Anthropol.* 30(3), 185–198.

Karakostis, F.A., Hotz, G., Scherf, H., Wahl, J., Harvati, K., 2017. Occupational manual activity is reflected on the patterns among hand entheses. *Am. J. Phys. Anthropol.* 164(1), 30–40.

Karakostis, F.A., Hotz, G., Scherf, H., Wahl, J., Harvati, K., 2018. A repeatable geometric morphometric approach to the analysis of hand entheseal three-dimensinal form. *Am. J. Phys. Anthropol.* 166(1), 246–260.

Karakostis, F.A., Jeffery, N., Harvati, K., 2019a. Experimental proof that multivariate patterns among muscle attachments (entheses) can reflect repetitive muscle use. *Sci. Rep.* 9, 16577.

Karakostis, F.A., Reyes-Centeno, H., Franken, M., Hotz, G., Rademaker, K., Harvati, K., 2020. Biocultural evidence of precise manual activities in an Early Holocene individual of the high-altitude Peruvian Andes. *Am. J. Phys. Anthropol.* 174(1), 35–48.

Karakostis, F.A., Wallace, I.J., Konow, N., Harvati, K., 2019b. Experimental evidence that physical activity affects the multivariate associations among muscle attachments (entheses). *J. Exp. Biol.* 222(23), jeb213058.

Kivell, T.L., 2015. Evidence in hand: recent discoveries and the early evolution of human manual manipulation. *Phil. Trans. R. Soc. B* 370(1682), 20150105.

Maki, J., Trinkaus, E., 2011. Opponens pollicis mechanical effectiveness in Neandertals and early modern humans. *PaleoAnthropol.* 2011, 62–71.

Marchi, D., Proctor, D.J., Huston, E., Nicholas, C.L., Fischer, F., 2017. Morphological correlates of the first metacarpal proximal articular surface with manipulative capabilities in apes, humans and South African early hominins. *C. R. Palevol* 16(5–6), 645–654.

Marzke, M.W., Tocheri, M.W., Steinberg, B., Femiani, J.D., Reece, S.P., Linscheid, R.L., Orr, C.M., Marzke, R.F., 2010. Comparative 3D quantitative analyses of trapeziometacarpal joint surface curvatures among living catarrhines and fossil hominins. *Am. J. Phys. Anthropol.* 141(1), 38–51.

R Core Team, 2021. *R: A Language and Environment for Statistical Computing*. R Foundation for Statistical Computing, Vienna.

Ruff, C., Holt, B., Trinkaus, E., 2006. Who's afraid of the big bad Wolff?: "Wolff's law" and bone functional adaptation. *Am. J. Phys. Anthropol.* 129(4), 484–498.

Singleton, M., 2002. Patterns of cranial shape variation in the Papionini (Primates: Cercopithecinae). *J. Hum. Evol.* 42(5), 547–578.

Tocheri, M.W., Orr, C.M., Jacofsky, M.C., Marzke, M.W., 2008. The evolutionary history of the hominin hand since the last common ancestor of *Pan* and *Homo*. *J. Anat.* 212(4), 544–562.

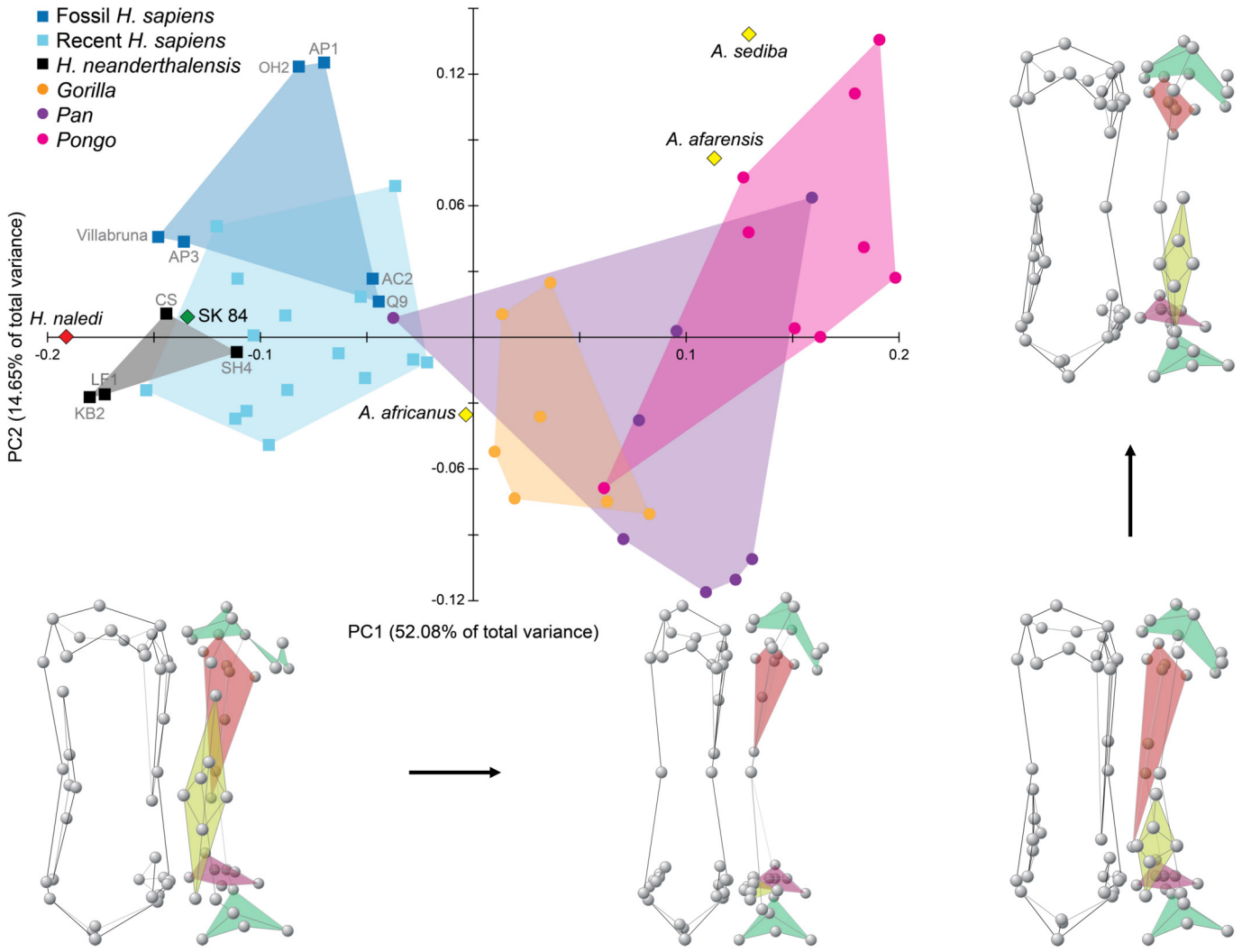

SOM Figure 1. PCA of Procrustes-superimposed landmarks of the first metacarpal without a priori *group association, PC1 compared to PC2. Shape changes along PC1 and PC2 are illustrated below and to the right of the plot, respectively. OP: red; DI1: yellow; APL: purple; articular surfaces: green. Abbreviations: OH: Ohalo; AP: Abrí Pataud; AC: Arene Candide; Q: Qafzeh; KB: Kebara; CS: Chapelle-aux-Saints; LF: La Ferrassie; SH: Shanidar.*

SOM TABLE 1. DESCRIPTIVE STATISTICS FOR THE SIZE-ADJUSTED ENTHESEAL SURFACE AREA MEASUREMENTS.

		OP	APL	DI1
Modern *H. sapiens* (n=15)	Mean	1.227	0.618	1.346
	SD	0.149	0.074	0.173
Fossil *H. sapiens* (n=6)	Mean	1.292	0.564	1.442
	SD	0.304	0.130	0.117
***H. neanderthalensis* (n=5)**	Mean	1.508	0.546	1.242
	SD	0.184	0.090	0.156
***Gorilla* (n=7)**	Mean	2.100	0.657	0.789
	SD	0.608	0.163	0.154
***Pan* (n=9)**	Mean	1.988	0.771	0.706
	SD	0.499	0.070	0.226
***Pongo* (n=9)**	Mean	1.503	1.104	0.690
	SD	0.484	0.334	0.216

SOM TABLE 2. STATISTICS OF THE DISCRIMINANT FUNCTION ANALYSIS.

DFA	Later *Homo**	Great apes*	Group centroid†
Entheseal patterns	100/100	96/96	1.66/-1.73

*% of original / cross-validated grouped cases correctly classified. Later *Homo* includes *H. sapiens* and *H. neanderthalensis.*

†*H. sapiens* and *H. neanderthalensis* / great apes.

SOM TABLE 3. CANONICAL DISCRIMINANT FUNCTION COEFFICIENT OF THE DISCRIMINANT FUNCTION ANALYSIS.

	Entheseal patterns
DI1	5.43
Constant	-5.67

SOM TABLE 4. LANDMARK DESCRIPTION FOR THE SHAPE ANALYSIS.

Landmark	Structure	Orientation	Landmark description
O1	OP	Lateral view	Most distal point of the enthesis
O2			Most palmar point in the area of the head (not the ridge)
O3			Most dorsal point in the area of the head (not ridge)
O4			Most proximal point of the enthesis
O5			App. Midpoint between points O2 and 3
O6			Midpoint along a virtual line that halves the OP ridge
A1	APL	Lateral view	Most palmar point on the proximo-palmar end of the enthesis
A2			Most dorsal point
A3			Most distal point
A4			Point on proximal border with app. equal distance to most palmar and most dorsal point of enthesis
A5&A6			Two equidistant points between A1 and 2, but projected onto most laterally elevated ridge
D1	DI1	Medial view	Most distal point on enthesis
D2			Midpoint on vertical line from landmark D1 to proximal end of enthesis, projected onto dorsal border
D3			Corresponding point on palmar border
D4			Most proximal point on enthesis
D5&D6			Two equidistant points placed between D1 and 4
B1	Overall bone	Dorsal view	Most distal point of the head
B2			Most projecting point of medial epicondyle of the head
B3			Most projecting point of lateral epicondyle/OP attachment of the head
B4		Palmar view	Medial midpoint of the shaft
B5			Lateral midpoint of the shaft
B6			Most proximally projecting point of the base
B7			Most medially projecting point of base
B8			Most laterally projecting point of base/APL
B9		Dorsal view	Most proximally projecting point of the base
PA1	Proximal articular surface	Proximal view	App. midpoint of medial border of articular surface, often where it's curved most distally
PA2			App. midpoint of lateral border of articular surface, often where it's curved most distally
PA3		Medial view	Most distal point of base curvature
DA1	Distal articular surface	Distal view	Most dorsal point on medial half of art. surface
DA2			Most dorsal point on lateral half of art. surface
DA3			Approximate midpoint of medial border
DA4			Approximate midpoint of lateral border
DA5		Disto-palmar view	Most proximal point on palmar-radial condyle
DA6			Most proximal point on palmar-ulnar condyle
DA7			Point between DA5 and 6, most distally (or most palmarly) protruding point on middle of palmar articular ridge

SOM TABLE 5. EIGENVALUES OF PC1–3 OF THE SHAPE PRINCIPAL COMPONENT ANALYSIS.

Principal component	Eigenvalues	% of variance
PC1	0.013	52.08
PC2	0.004	14.65
PC3	0.002	7.28